processes

MDPI

Article

Design and Field Application of Staged Composite Slugs for Gas Channeling Control in Underground Gas Storage

Xida Zhou [1], Wenming Wu [1,*], Xiaocen Liu [2], Jie Yao [2] and Yufeng Zhao [3]

[1] Sanya Offshore Oil and Gas Research Institute, Northeast Petroleum University, Sanya 572025, China; zhouxida111@gmail.com
[2] Oil and Gas Production Management Area, PetroChina Tarim Oilfield Company, Korla 841000, China; lxcen-tlm@petrochina.com.cn (X.L.); yaojie-tlm@petrochina.com.cn (J.Y.)
[3] Shenzhen Greending New Energy Technology Development Co., Ltd., Shenzhen 518000, China; zhaoyufeng1985@outlook.com
* Correspondence: wwmlh10126@163.com

Abstract

The engineering problem in producer-side foam treatment is to retain placement access while developing sufficient flow resistance. This study integrates conventional and enhanced foaming fluids, a water spacer, imbibition fluid and light-oil displacement with explicit volume estimates and pressure-responsive injection. The novelty is field-scale process organization rather than new chemical development. Screening at 140 °C and 2.34×10^5 mg/L salinity supported initial concentrations of 1.0 wt% base formulation, 0.2 wt% xanthan gum and 1.5 wt% imbibition formulation. Single-core and parallel-core recovery gains were 13.64 and 21.95 percentage points. In pilot well P1, the three principal injected volumes were 287, 288 and 288.6 m3. Over 212 calendar days, oil production averaged 19.01 t/d and cumulative-production GOR was 1082.87 m3/t, 78.6% below the historical reference. Reference-equivalent incremental oil was 3167.88 t, varying from 2952.14 to 3311.71 t across ±20% baseline-GOR scenarios. The pilot demonstrates implementability; a single well without a matched control or downhole placement monitoring cannot establish comparative superiority or spatial slug boundaries.

Keywords: underground gas storage; gas channeling; staged foam placement; imbibition; treatment volume; surface pressure monitoring

Check for updates

Academic Editor: Qiang Yu

Received: 13 September 2026
Revised: 16 October 2026
Accepted: 26 October 2026
Published: 2 November 2026

Copyright: © 2026 by the authors. Licensee MDPI, Basel, Switzerland. This article is an open access article distributed under the terms and conditions of the Creative Commons Attribution (CC BY) license.

1. Introduction

Gas migration through preferential pathways can reduce effective sweep and increase the gas–oil ratio of producers in oil-reservoir areas undergoing conversion to underground gas storage. Injection–production management and chemical conformance control address different parts of this problem. Microscopic storage experiments have shown that operating rate affects gas–liquid displacement and pore-space use, while heterogeneous-core and field studies have examined water-alternating-gas and foam-assisted injection strategies [1–3]. For a mature horizontal producer, the practical task is to deliver treatment fluid into the relevant gas-entry region while retaining sufficient access to poorly swept oil-bearing intervals.

Published foam processes already include selective injection, staged gas shutoff and changes in surfactant delivery. Shojaiepour et al. considered injection location and scheduling in a reservoir simulation; Hassanzadeh et al. examined surfactant delivery with supercritical CO_2; Xiao et al. connected laboratory screening with a sandstone field pilot; and

Telin et al. applied a foam-gel sequence followed by hydrogel in horizontal producers [4–7]. Accordingly, staged injection itself is established practice. The unresolved issue addressed here is how to organize a producer-side sequence, estimate an executable fluid inventory and adapt pumping to the well response under the available field constraints.

Material screening alone does not resolve the balance between propagation and resistance. Polymer reinforcement can improve foam stability while changing foaming capacity and flow behavior, and methane foam performance depends on porous-medium conditions and oil contact [8–10]. Pore-scale research on reactive CO_2/N_2–CH_4 transport further illustrates that gas composition and pore geometry affect migration, although those reactive carbonate results do not directly define a treatment radius for the present sandstone well [11]. An engineering design must therefore distinguish a material property, a hypothesized placement mechanism and a field observation.

Previous screening and core-scale work do not by themselves specify a field liquid inventory, tubing displacement or a workable pressure-control procedure. This study addresses those scale-up tasks in producer P1 using conventional foaming fluid, enhanced foaming fluid, a formation-water spacer, imbibition fluid and light-oil displacement. The novelty is the integration of functional sequential placement with explicit volume assumptions and surface-pressure-responsive execution, rather than a new foaming chemical or the first use of staged foam. Direct single-core and parallel-core results are included here. Model forecasts, digitized traces and recorded field totals are identified separately; the pilot tests field implementability rather than comparative superiority under matched conditions.

2. Materials and Methods

2.1. Target Well and Fluid Properties

P1 is a screen-completed horizontal producer in the Carboniferous Donghe 1 reservoir pilot area. Well identifiers P1 and I1 are retained for the treated producer and associated gas injector. The completed measured-depth interval is 5864.62–6365.69 m, with 501.07 m of exposed screen. The 5852–5914 m interval identified in the geological interpretation has a measured-depth length of 62 m and intersects the completed interval over 49.38 m. Neither length represents vertical net pay.

The preferential gas-entry interval was selected by combining completion exposure, interpreted porosity and oil saturation, production deterioration and gas streamlines from the existing well-group model. Heel porosity reaches 17.3% and interpreted oil saturation is about 62%; a representative middle-to-distal porosity is 12.7%, with poorer intervals at 9.5–11.0% and oil saturation around 52% in the principal oil-bearing section [12,13] The well and fluid information, together with the relevant measurement context, is summarized in Table 1.

Table 1. Well and fluid information with measurement context.

Parameter	Value
Horizontal-end TVD	5742.13/5743.26 m
Interpreted gas-entry interval	5852–5914 m MD
Porosity	17.3%
Pressure reference	60 MPa
Evaluation temperature	140 °C
Evaluation-brine salinity	2.34×10^5 mg/L
Historical water salinity	$(1.464–1.824) \times 10^5$ mg/L
Oil density	0.838 g/cm^3 at 20 °C; 0.8165 g/cm^3 at 50 °C
Reported oil viscosity	3.307 mPa·s
Methane content	82.66–85.69%
Displacement-oil density	approximately 0.85 g/cm^3

2.2. Staged Treatment Design

The field process uses aqueous foaming solutions that are intended to generate foam on contact with formation natural gas; field quantities are liquid preparation volumes, not expanded in situ foam volumes. The initial conventional formulation is APG0810 and DAB35 at a 1:1 mass ratio and 1.0 wt% total prepared formulation. The enhanced fluid contains the same base formulation and 0.2 wt% xanthan gum. The imbibition formulation is a bio-based surfactant blend used at 1.5 wt%. Concentrations follow the preparation records and are mass fractions; an independently measured active-content correction was not available. No crosslinked gel was injected in this job.

The leading conventional fluid is intended to provide access before a more stable foam structure develops; the enhanced fluid follows to increase the persistence of flow resistance. A 5 m^3 formation-water spacer reduces direct mixing in the tubing between enhanced and imbibition fluids, but cannot guarantee chemically isolated fronts underground. The imbibition fluid then targets oil mobilization under the altered flow conditions. Light oil displaces the chemical inventory out of the tubing and limits the final additional water load. Its lower liquid-column density is favorable for unloading, although oil contact can weaken foam and therefore requires control of overdisplacement [7–10]. Figure 1 summarizes the sequence; planned and actual liquid volumes are reported in Table 2.

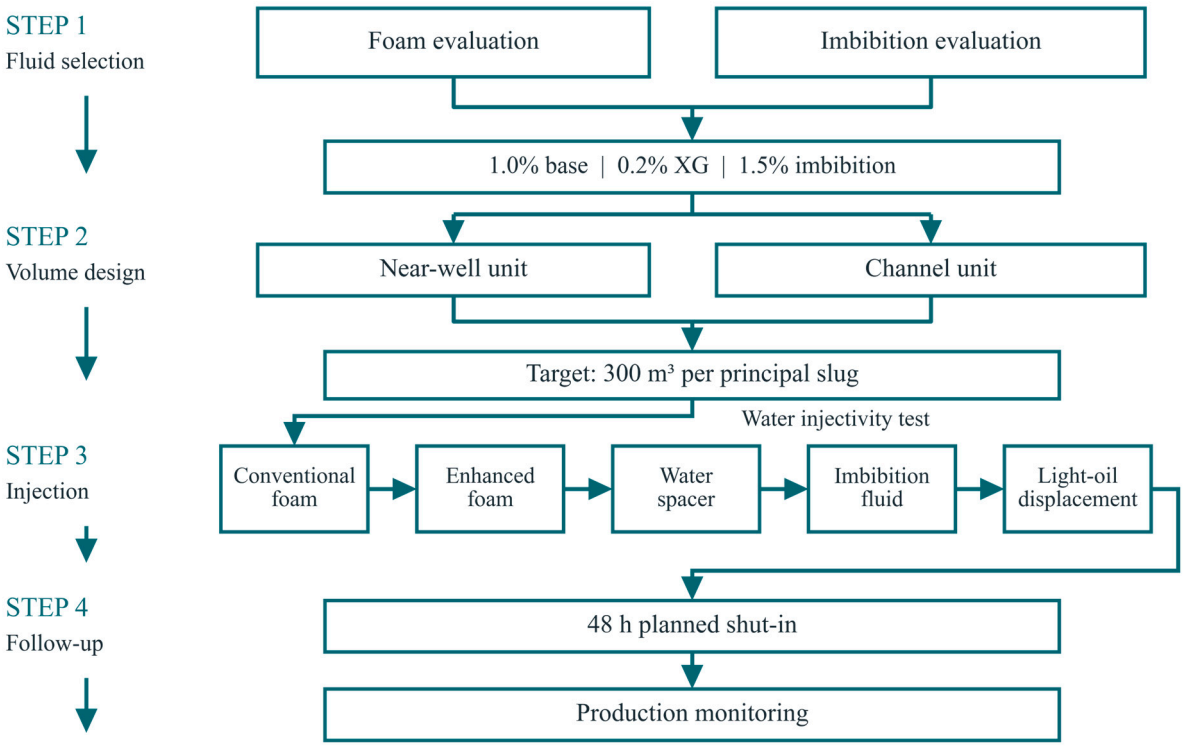


Figure 1. Process design and execution workflow. Fluid selection and equivalent-volume design precede the five-stage injection sequence; shut-in and production monitoring follow displacement.

A simplified parallel-path argument explains the expected redistribution. If branch j has hydraulic conductance Cj, and both branches experience the same pressure difference, the low-conductance branch receives the fraction given by Equation (4). Reducing the effective gas conductance of the preferential branch can increase the fractional access to the poorer branch, provided entry pressure and connected oil-volume permit flow. The relevant change is in effective multiphase mobility, not necessarily intrinsic rock permeability. This conditional mechanism does not prove the locations of individual slugs. Mixing the two formulations is physically possible; the sequential design preserves a lower-reinforcement

leading fluid and a more stable trailing fluid. A matched total-dose sequential-versus-mixed comparison was not performed, so a unique optimum sequence cannot be inferred.

Table 2. Estimated planned and injected liquid volumes.

Fluid	Estimated m^3	Planned m^3	Injected m^3
Conventional foaming fluid	313.38	300	287
Enhanced foaming fluid	278.56	300	288
Water spacer	Execution allocation	5	5
Imbibition fluid	174.10 + 139.58 = 313.68	300	288.6
Light-oil displacement	45.11 + approximately 10	55	62.8
Water injectivity test	Separate injectivity step	20	30

The order addresses an access–resistance trade-off. Placing the enhanced formulation first could establish resistance in the first contacted region before sufficient liquid enters the intended treatment interval. A conventional leading fluid preserves an initial placement opportunity, while the enhanced trailing fluid is intended to maintain the resistance developed along accessible paths. The spacer then separates the main chemical inventories in the tubing before the mobilization fluid is delivered. These are design reasons for the selected order; the present corefloods evaluate the resulting combination and do not determine the response of a reversed or premixed sequence.

2.3. Treatment-Volume Design and Wellbore Displacement

The volume estimate is an engineering construction from an equivalent bulk-volume term, a representative porosity and an effective liquid-allocation factor. It is not a first-principles solution for foam propagation. Figure 2 distinguishes the full completed interval from the interpreted gas-entry region. The near-wellbore and channel terms can overlap physically; their sum is a bookkeeping allocation for a preparation inventory rather than a measurement of two disjoint pore volumes. The adopted expression is

$$Q = \frac{4}{3}\pi {d_1}^2 \times L_1 \times \phi_1 \times A + \frac{4}{3}\pi {r_2}^2 \times L_{2,i} \times \phi_2 \times B \quad (1)$$

Equation (1) is constructed by multiplying an equivalent cross-sectional area by an axial allocation length, porosity and a liquid-allocation fraction. The near-well area term is $\pi {d_1}^2$ and the channel receiving-area term is $\pi {r_2}^2$; multiplication by L_1 and $L_{2,i}$ gives bulk-volume terms in m^3. Multiplication by ϕ_1 A and ϕ_2 B assigns liquid inventory to those terms. The common multiplier 4/3 is an inherited engineering coefficient applied to these equivalent units. This construction explains the dimensional form without treating the coefficient as a transport law or deriving a spherical treatment boundary.

Here, $d_1 = r_1 - r_w$ is the equivalent radial scale used in the original design; r_1 is the outer radial coordinate and r_w is the wellbore radius. It is an equivalent radial scale, not the annular-area expression ${r_1}^2 - r_w^2$. L_1 is the treated completion length, r_2 is the equivalent receiving-area radius and $L_{2,i}$ is a fluid-specific allocation depth. A and B are dimensionless effective filling/allocation factors for the near-wellbore and channel contributions. Both are 0.50 in the inherited design. The common geometric factor 4/3 is retained from the field design and is written explicitly in Equations (1) and (2). Neither the 0.50 factors nor the 4/3 factors were independently calibrated by this coreflood program. A and B do not represent laboratory plugging efficiency, measured channel occupancy or fitted recovery multipliers. All length terms are in metres and porosity enters as a fraction, giving Q in cubic metres.

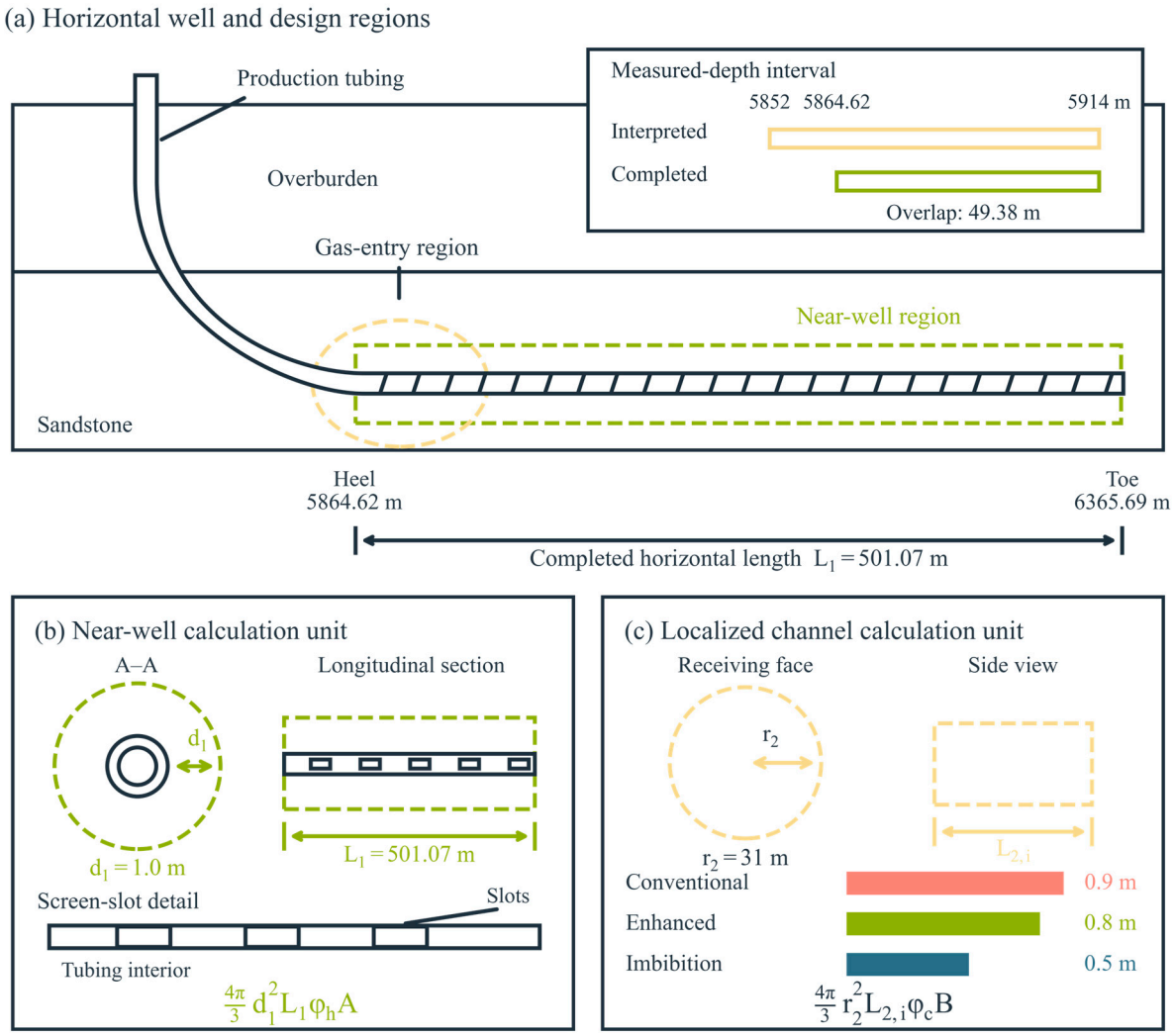


Figure 2. Horizontal completion and equivalent units for volume estimation. The near-well cross-section, screen-slot detail and localized-channel allocation depths are schematic design quantities.

For conventional and enhanced foaming fluids, only the channel contribution is allocated in the adopted inventory design. Subscript f denotes either foaming fluid, with $L_{2,f}$ equal to 0.9 or 0.8 m, respectively. Omitting a separate near-well inventory term does not imply that foam cannot enter the near-well region:

$$Q_f = \frac{4}{3}\pi r_2^2 \times L_{2,f} \times \phi_2 \times B \quad (2)$$

Because A and B multiply their respective contributions directly, they control assigned inventory rather than measured blocking efficiency. For example, reducing B from 0.50 to 0.45 lowers the conventional-fluid estimate by 10%, with all other inputs fixed. Equal numerical values of A and B do not imply identical physical occupancy in the two regions. A future calibration would require an independent placement constraint, such as tracer-resolved arrival or a measured intake profile; fitting either factor to the same post-treatment oil total would confound placement with the production response.

The conventional-foam example gives $Q = (4/3)\pi \times 31^2 \times 0.9 \times 0.173 \times 0.50 = 313.38$ m^3. The corresponding enhanced-foam estimate is 278.56 m^3. The imbibition estimate is 174.10 m^3 for the channel contribution plus 139.58 m^3 for the near-wellbore contribution, totaling 313.68 m^3. Using π at full numerical precision rather than the earlier design approximation of 3.14 changes these estimates by less than 0.1%. All three were planned at 300 m^3

to match field preparation and execution. The differences from the estimates are −4.27%, +7.70% and −4.36%, respectively. These deviations are reported explicitly; rounding is an execution choice within an empirical design, not evidence that treatment performance is insensitive to volume.

At a baseline conventional-foam volume of 313.38 m^3, varying r_2 alone by −10% or +10% gives 253.84 and 379.19 m^3, corresponding to −19% and +21%. The linear factors L_2, ϕ_2 and B each produce a ±10% volume change when varied separately (Figure 3). The differential form is Equation (3). This calculation concerns uncertainty in the estimated liquid inventory. It does not quantify uncertainty in recovery or in an underground treatment radius. Adsorption-aware foam optimization and reservoir-scale studies require additional transport, pressure and economic constraints that are outside this simple expression [14–16].

$$\frac{\Delta Q}{Q} \approx 2\frac{\Delta r_2}{r_2} + \frac{\Delta L_2}{L_2} + \frac{\Delta \phi_2}{\phi_2} + \frac{\Delta B}{B} \quad (3)$$

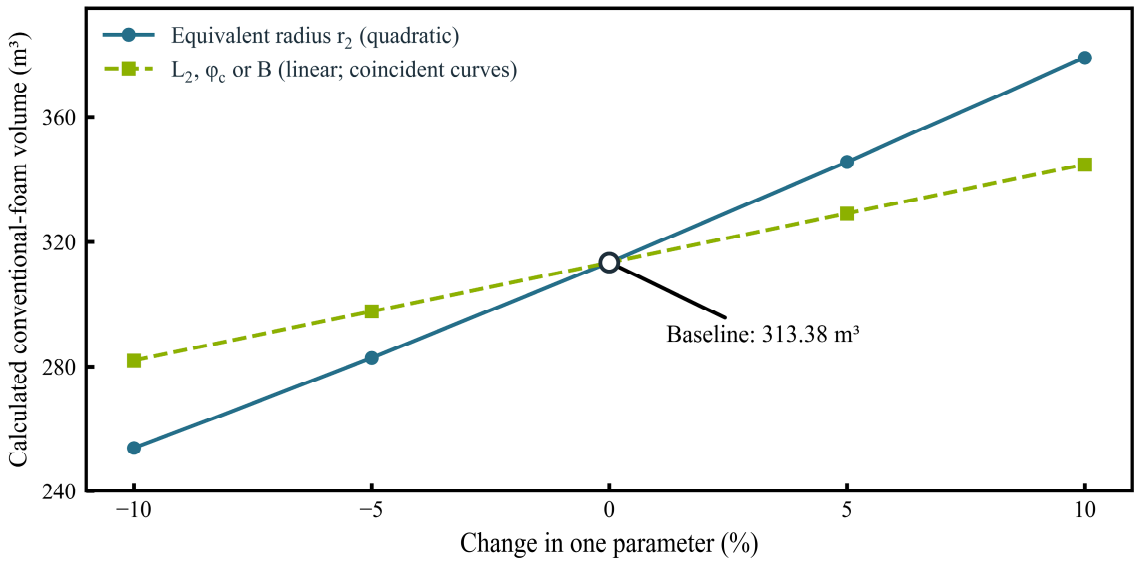


Figure 3. One-at-a-time sensitivity of calculated conventional-foam volume. The linear curves for L_2, φ_2 and B coincide.

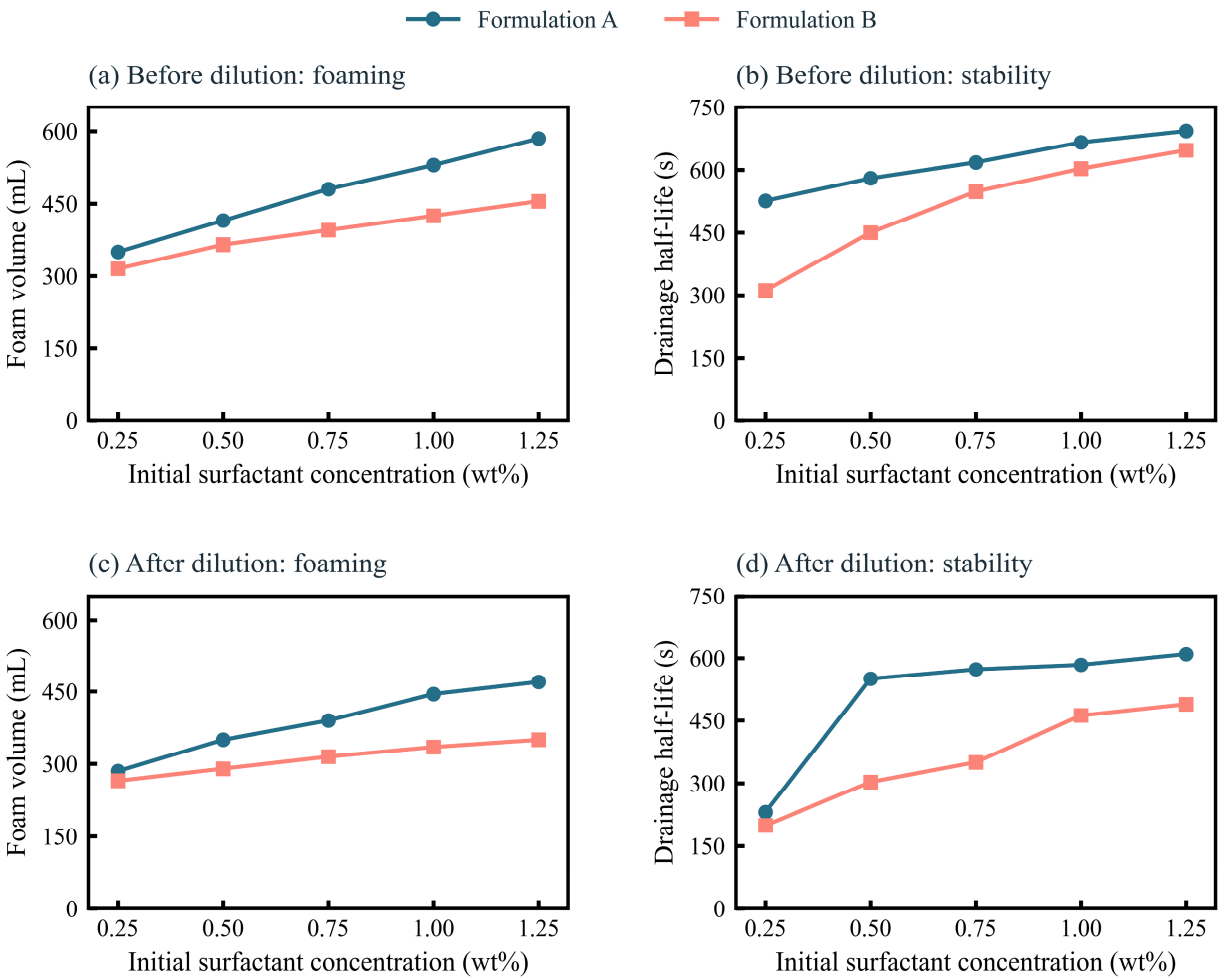
The estimate is appropriate as an initial inventory calculation for a screen-completed producer with an interpretable preferential gas-entry region and sufficient injectivity. Reuse requires reassessing geometry, fluid properties, overlap and allocation factors. The present coefficients and 300 m^3 principal-slug volume should not be transferred directly to wells dominated by large open fractures, caves, unisolated crossflow or markedly different completion exposure. They also cannot replace a fracture-pressure or well-integrity assessment.

2.4. Fluid Evaluation and Coreflood Procedures

For the base-foam comparison, formulations A (APG0810/DAB35) and B (APG1214/DAB35), each at a 1:1 mass ratio, were prepared at initial concentrations of 0.25–1.25 wt%. Samples were aged at 140 °C for 14 days, agitated at 6000 r/min for 5 min and characterized by foam volume and drainage half-life. A separate 1:1 dilution with formation water reduced the nominal concentration to half its initial value. Concentration labels in Figure 4A therefore denote the prepared concentration before dilution. The enhancer comparison used a separate 140 °C, 24 h aging protocol and 0–0.5 wt% XG. Its half-lives cannot be used as a direct comparison of 14-day material lifetime. Static screening supports formulation choice but does not substitute for a dynamic gas-blocking test [17].

The imbibition evaluation used reservoir plugs that were dried, evacuated, saturated with water and then with oil according to the preparation records. Fluids at 1.0–3.0 wt% were examined for surface and oil–water interfacial tension and for oil release during 48 h at 140 °C. The plug set spans 0.061–6.045 mD and differs among concentrations; the 1.5 wt% outcome is therefore a formulation-selection result rather than an isolated concentration effect on identical plugs. Interfacial tension is interpreted together with the recovery response, consistent with the need to consider wettability and capillary conditions [18].

Single-core and parallel-core tests used N_2 as the model gas, a nominal injection rate of 0.05 mL/min, 140 °C and the reported 60 MPa reservoir-condition input. Laboratory foaming solutions used the 0.5 wt% base system and the XG-enhanced formulation from the preparation record; these concentrations are distinguished from the 1.0 wt% initial field recipe. The plug properties used in dynamic tests are listed in Table 3. After the first forward gasflood reached severe channeling and negligible oil production, fluids were introduced in reverse from the production end. The single-core treatment comprised 0.5 PV of conventional and 0.5 PV of enhanced fluid. The parallel test additionally used a 0.1 PV spacer and 0.5 PV imbibition fluid. Both tests were shut in for 30 min before forward gasflooding resumed. PV denotes the pore-volume basis for the corresponding core system. Plotted cumulative coordinates follow the reported gasflood series; treatment-liquid PV is specified separately. Field liquid volumes are not scaled directly from these PV ratios.



(**A**)

Figure 4. *Cont.*

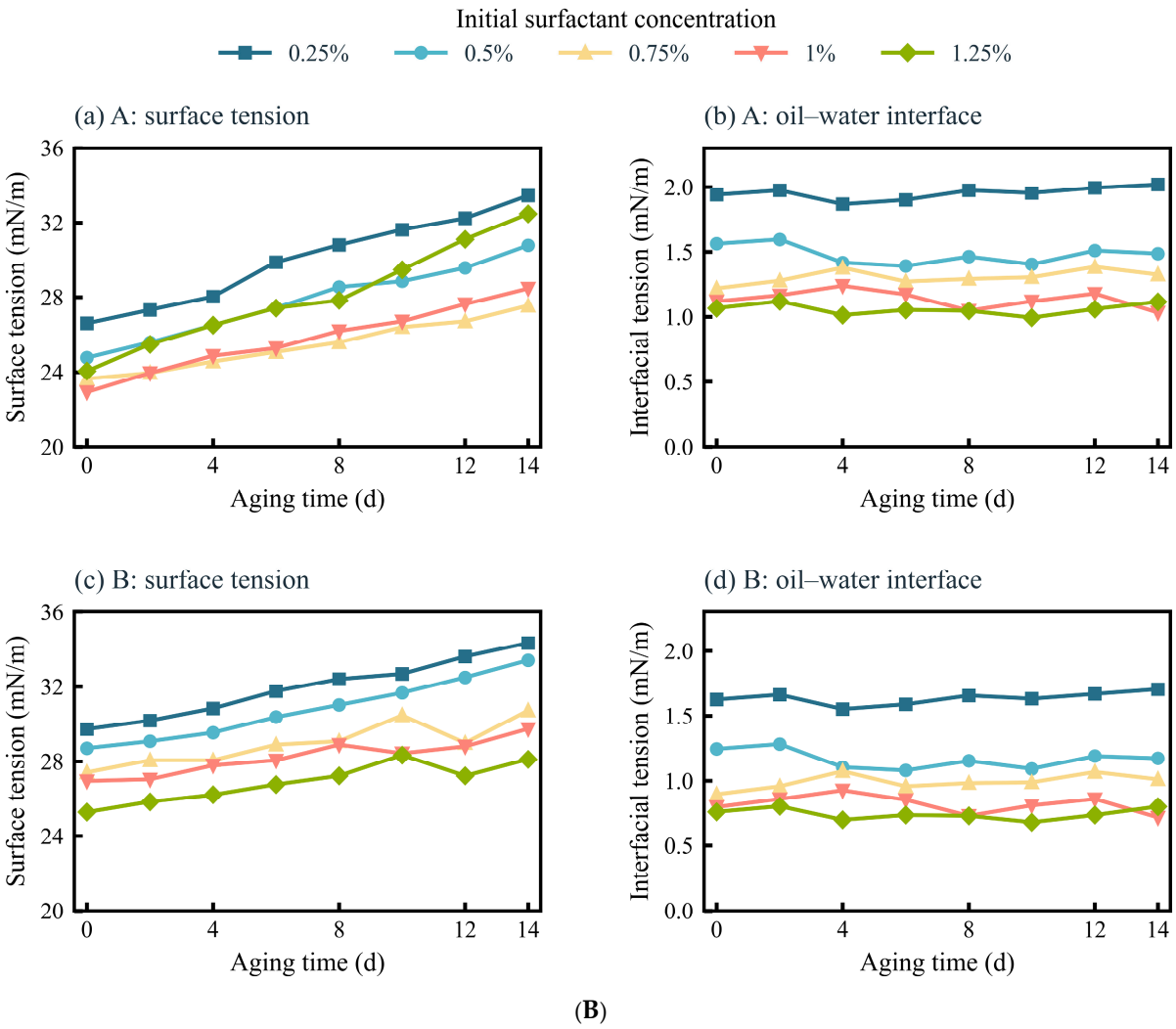


Figure 4. (**A**) Foam volume and drainage half-life of formulations A and B after 140 °C aging for 14 days, before and after 1:1 dilution. The *x*-axis gives the initial mass fraction. (**B**) Surface- and oil–water interfacial-tension trends for diluted formulations A and B.

Table 3. Core properties used in dynamic tests.

Core Role	Length (mm)	Diameter (mm)	Porosity (%)	Permeability (mD)
H and single core 1	55.365	24.785	17.100	6.045
L branch 2	46.385	24.680	14.169	1.148

Recovery is cumulative produced oil divided by initial oil in the relevant core or combined system; total recovery is not the unweighted mean of the two branch percentages. Laboratory gas–oil ratios use oil volume, whereas field gas–oil ratios use oil mass. The single-core and parallel-core records are individual validation runs.

2.5. Model Cases and Evaluation Metrics

The supporting single-core model used a 5 × 20 × 1 grid; the parallel-core model used an 11 × 20 × 1 layout with inactive separating cells. The supplied study introduced a twofold-permeability streak and inherited relative-permeability and PVT descriptions from the block model. The recorded single-core modeled recoveries before and after treatment

were 36.88% and 48.47%, compared with measured values of 38.63% and 52.27%. These correspond to differences of 1.75 and 3.80 percentage points.

Five well-group design cases assigned equal liquid volumes of 100, 200, 300, 400 or 500 m^3 to the conventional, enhanced and imbibition principal slugs. The existing reservoir model was history matched through December 2024 and was forecast over 2025–2029, with the first production year used for case comparison. The inherited schedule includes interruption of gas injection at I_1, a model treatment/shut-in period and restart at reference operating rates. This schedule differs from the 48 h field shut-in. Consequently, the one-year oil-volume forecasts are conditional comparisons among model cases; they are not a prediction of the exact 212-day field response or a comparison in tonnes with the historical-GOR accounting result.

For an idealized parallel system, the conductance relation used to interpret possible redistribution is

$$C_j = \frac{k_j \times k_{r,j} \times A_{c,j}}{\mu_j L_j}, f_L = \frac{C_L}{C_H + C_L} \quad (4)$$

For field pressure interpretation, a single-phase bookkeeping relation is

$$P_{bh} = P_{surf} + \rho g H - \mathbf{\Delta} P_{fric} \quad (5)$$

Bottomhole pressure equals surface tubing pressure plus hydrostatic head minus frictional loss in this simplified relation. Multiphase flow, changing density, gas generation and tubing geometry add uncertainty. The available surface traces do not provide the measurements needed to separate those terms quantitatively; they are used to describe operational response, not to calculate a unique formation resistance factor. Liquid injectivity in foam processes depends on permeability and the prior gas–liquid state, reinforcing the need to interpret rate and pressure jointly [19].

H in Equation (5) is the vertical liquid-column height relevant to the pressure measurement. It is distinct from measured depth and the 501.07 m horizontal completion length. The approximately 5743 m true vertical depth in Table 1 illustrates why hydrostatic head matters, but a defensible correction still requires the fluid density distribution and flowing conditions at each stage. The 60 MPa reservoir-condition input and the 30 MPa surface warning therefore refer to different locations and purposes and are not directly compared as equivalent pressure limits.

3. Laboratory Results and Model Based Design

3.1. Selection of Working Concentrations

The numerical base-foam dataset is shown in Figure 4A. At an initial formulation-A concentration of 1.0 wt%, the aged sample produced 530 mL of foam with a drainage half-life of 666 s before dilution; after 1:1 dilution to 0.5 wt%, the values were 445 mL and 584 s. At an initial concentration of 0.5 wt%, the corresponding diluted sample was at 0.25 wt%, with 350 mL and 550 s. These are different points and are not interchanged. Increasing the initial concentration from 1.0 to 1.25 wt% yielded diluted-sample values of 470 mL and 610 s. The moderate additional response, together with formulation consumption and dilution allowance, supported the 1.0 wt% field choice. Without a replicated cost–response optimization, it is an engineering selection rather than a statistically established optimum.

The marginal comparison is relevant to that choice. Increasing initial formulation A from 1.0 to 1.25 wt% requires 25% more formulated material at a fixed prepared-fluid volume. After dilution, foam volume increases from 445 to 470 mL, or 5.62%, and half-life increases from 584 to 610 s, or 4.45%.

Figure 4B retains the aging-related surface- and interfacial-tension trends of the diluted samples. At 14 days, formulation A prepared initially at 1.0 wt% had a surface tension of 28.47 mN/m and an oil–water interfacial tension of 1.032 mN/m.

Under the separate 24 h enhancer protocol, the diluted base sample gave 455 mL and 612 s. With 0.2 wt% initial XG, it gave 380 mL and 2263 s: a 3.70-fold half-life and a 16.5% decrease in foaming volume relative to that control. The undiluted 0.2 wt% sample gave 420 mL and 4295 s. Figure 5 shows the broader stability–foaming trade-off.

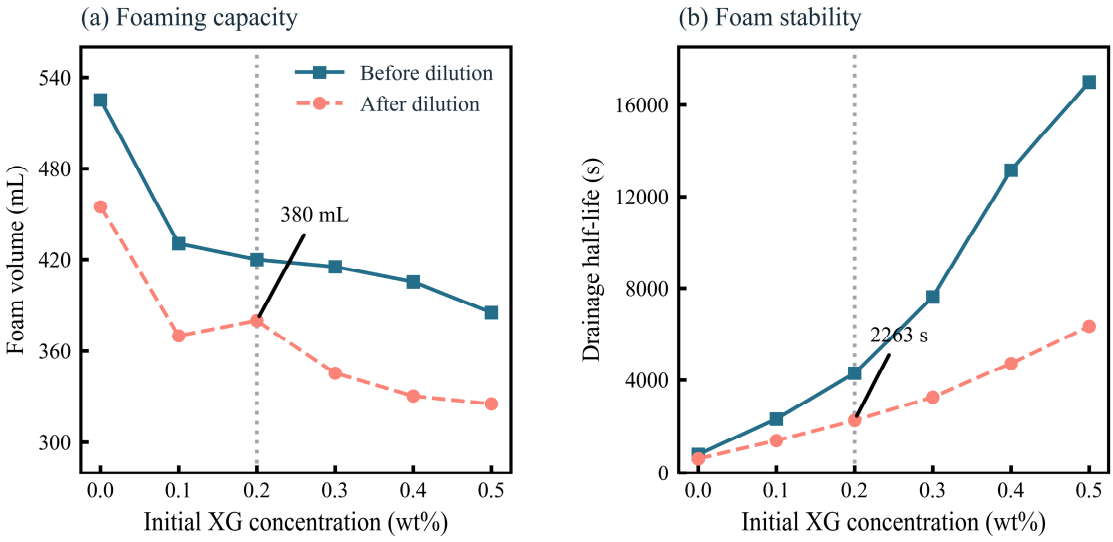


Figure 5. XG effects on foaming volume and drainage half-life under the 140 °C, 24 h protocol.

At 1.5 wt%, the imbibition fluid had a surface tension of 24.27 mN/m and an oil–water interfacial tension of 0.236 mN/m; the associated 48 h recovery was 36.76% (Figure 6). Raising the concentration reduced interfacial tension further in parts of the tested range but did not produce a uniformly higher imbibition response. Because plug properties differed, this observation cannot isolate the separate effects of concentration, pore structure and initial saturation. The 1.5 wt% selection is supported by the observed response and lower formulation inventory relative to higher-concentration recipes.

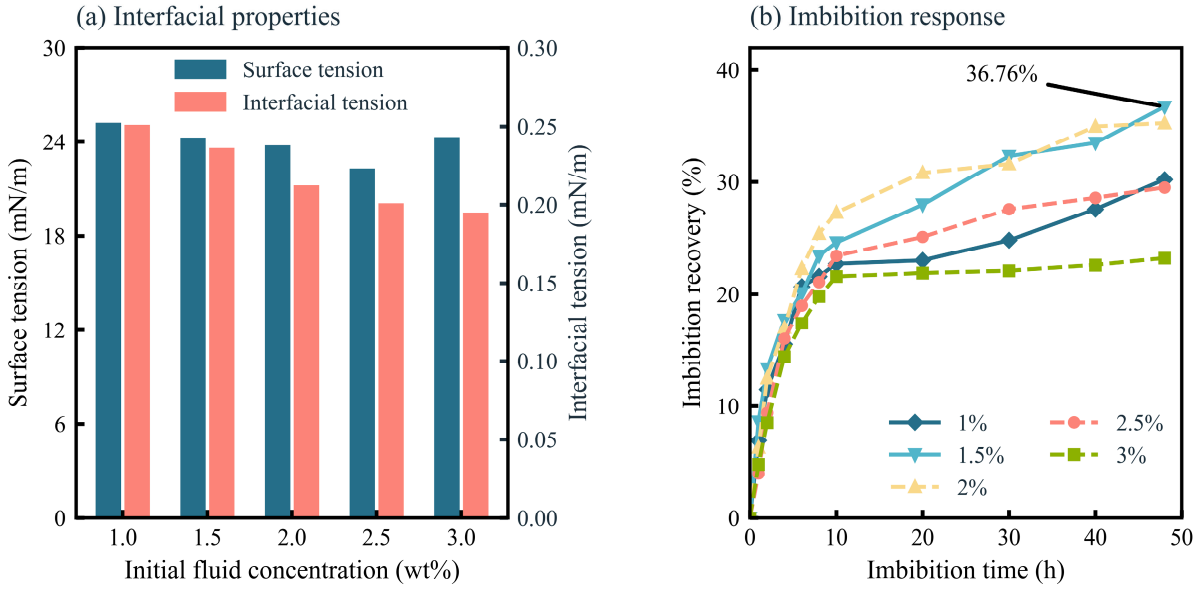


Figure 6. Interfacial properties and imbibition responses.

3.2. Single-Core Response

In the single core, first gas breakthrough occurred at approximately 0.7 PV. Severe channeling developed near 1.9 PV, when cumulative oil recovery was 38.63%. After reverse injection of conventional and enhanced fluids and a 30 min shut-in, the subsequent gasflood showed a larger pressure response and further oil recovery. Final cumulative recovery was 52.27%, a gain of 13.64 percentage points (Figure 7). The later cumulative-volume coordinate of 3.70 PV is reported as an endpoint, not as a newly identified second-breakthrough volume. The pressure and gas–oil ratio trajectories support a change in core-scale flow behavior after treatment; they do not separate the individual contributions of the two formulations.

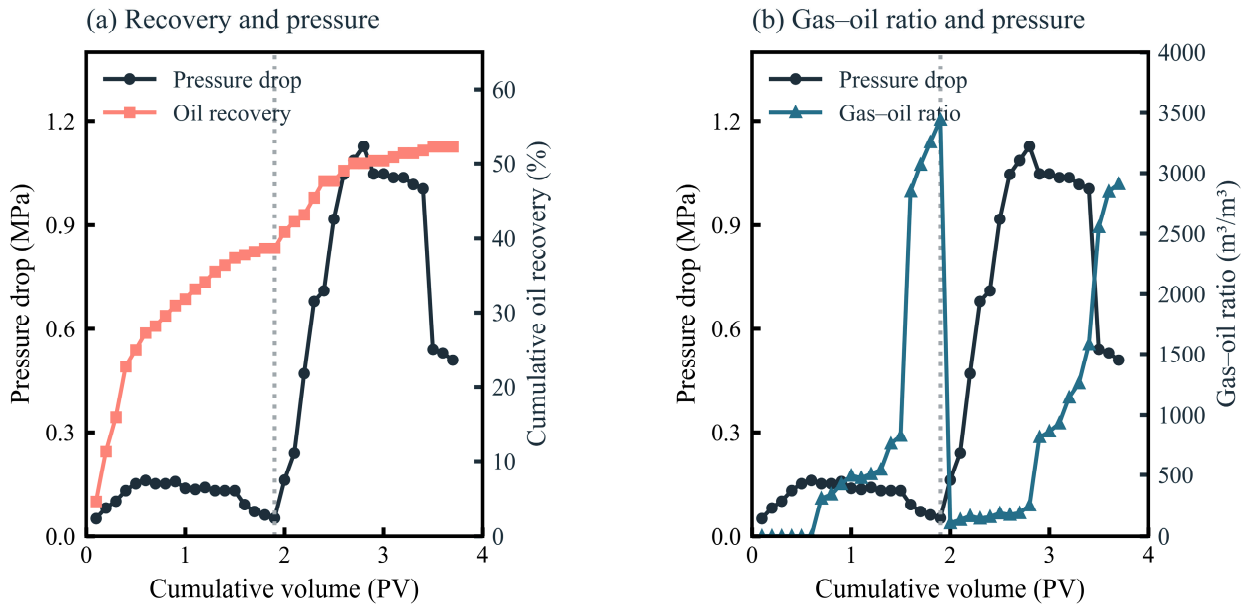


Figure 7. Single-core pressure drop, recovery and gas–oil ratio.

3.3. Parallel-Core Response

The parallel system had permeabilities of 6.045 and 1.148 mD, a ratio of 5.26. Before treatment, appreciable oil production came from the H branch; its recovery reached 31.81%, and system recovery was 19.44%. After the composite sequence, the L branch began producing oil at the reported cumulative coordinate of about 2.25 PV. Its gas appeared near 3.25 PV. Final H-branch, L-branch and system recoveries were 43.18%, 38.57% and 41.39%, respectively (Figure 8). The system increase was 21.95 percentage points. The appearance of additional L-branch oil is consistent with access to previously poorly swept pore volume, while common pressure and changing gas–oil ratios provide supporting dynamic context.

The system recovery must be weighted by the initial oil inventory of the two plugs. The branch difference also means that a total gas–oil ratio can fall as low-GOR oil from the poorer branch contributes, even when gas flow in the preferential branch remains significant. These results support a redistribution interpretation under the laboratory conditions. However, branch liquid allocation during treatment, direct foam-front images and an equal-dose single-slug control were not measured. The tests therefore support the feasibility of the combination without proving a unique spatial order, a recovery advantage over co-injection or a field-scale recovery multiplier. Coreflood selectivity and foam/gel studies provide context for heterogeneity-dependent resistance [20–22]. Studies of combined profile control and gas-injection schedules also treat sequence and cycling as design choices [23–25]. Their media and operating conditions differ from those used here.

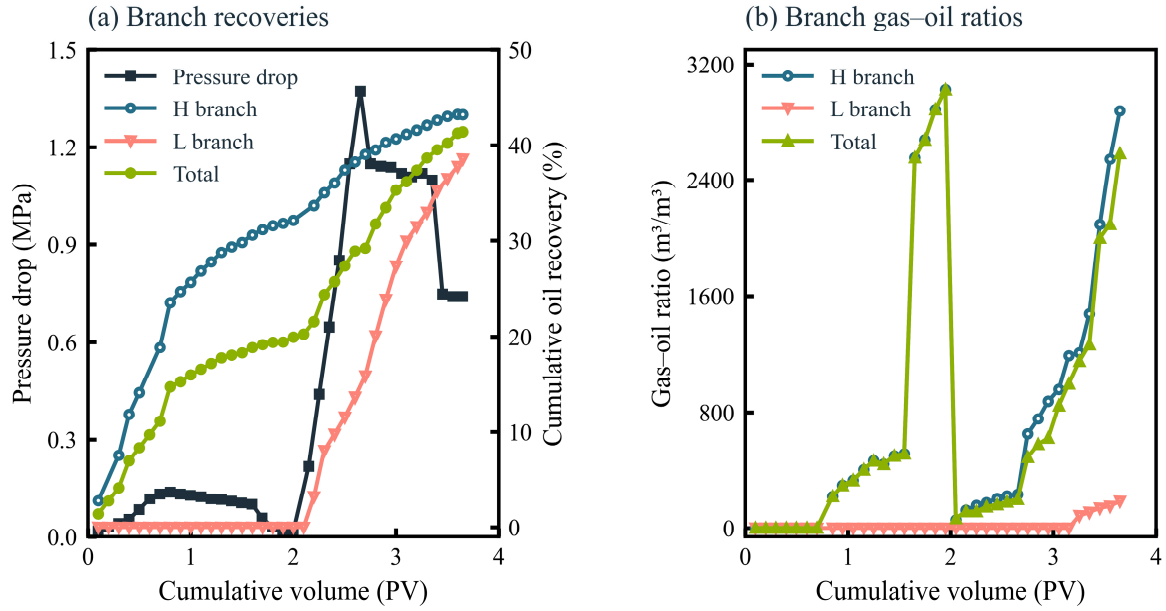


Figure 8. Parallel-core branch recoveries, system pressure drop and branch gas–oil ratios. H and L denote higher- and lower-permeability branches.

3.4. Volume Case Comparison

The model predicted one-year incremental oil volumes of 172, 564, 1253, 1368 and 1427 m^3 for equal principal-slug volumes of 100, 200, 300, 400 and 500 m^3, respectively (Figure 9). Increasing each slug from 300 to 400 m^3 adds 300 m^3 of total principal liquid for 115 m^3 more predicted oil; increasing from 400 to 500 m^3 adds another 300 m^3 for 59 m^3 more predicted oil. The corresponding oil-volume gains are 9.18% and 4.31%. The 300 m^3 case therefore offers a practical point before the modeled marginal response becomes smaller. Without actual chemical costs, matched pressure constraints and uncertainty propagation, it cannot be called a demonstrated economic optimum.

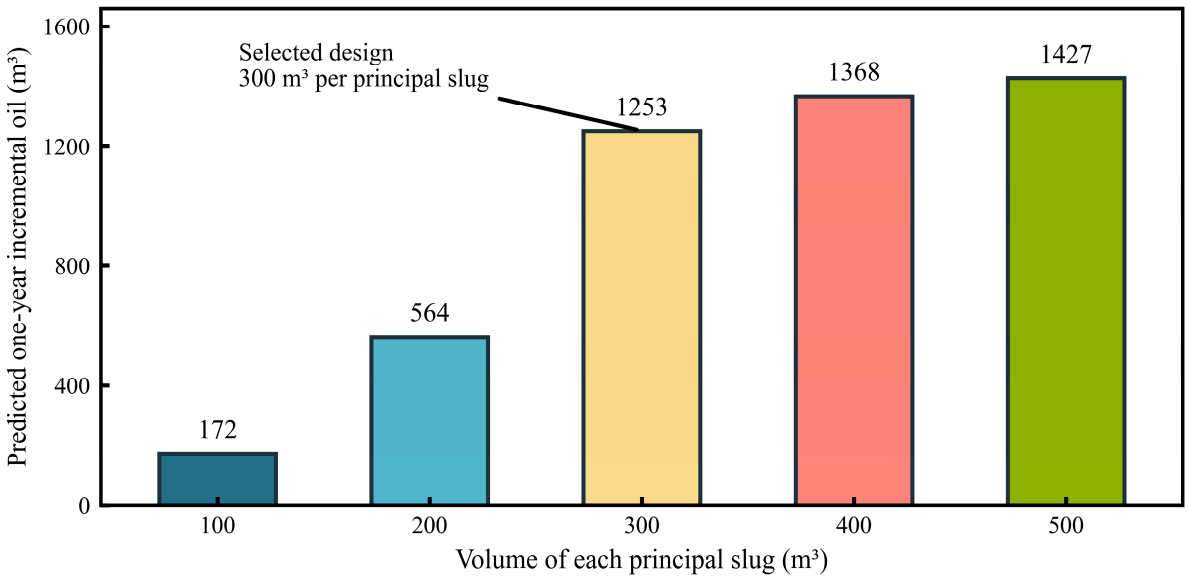


Figure 9. One-year incremental oil-volume predictions for five equal-principal-slug model cases. The values are conditional model forecasts, not measured field increments.

4. Field Implementation and Production Evaluation

4.1. Execution and Measurement Locations

The job was performed on 27–29 October 2025 through the existing tubing of P_1. I_1 was the associated gas injector used in the well-group interpretation; it did not receive this chemical job. The water injectivity test used 30 m^3. Subsequent conventional, enhanced, spacer, imbibition and light-oil volumes were 287, 288, 5, 288.6 and 62.8 m^3, totaling 931.4 m^3 excluding test water. With a tubing internal volume of 45.11 m^3, the actual light-oil overdisplacement was approximately 17.69 m^3. A 48 h shut-in was planned after displacement. Production restart also required unloading and gas lift, which must be considered in interpreting the later production response.

Pump pressure, tubing pressure, casing pressure and the separately recorded B-annulus pressure are surface channels. B designates the monitored annulus compartment in the job record; it is not a downhole formation-pressure sensor and is not interchangeable with the casing-pressure curve. The supplied record does not establish the full annular isolation geometry or an independently verified absolute-pressure datum, so no conversion of annulus pressure to formation pressure is attempted. Figure 10 identifies the treated producer and surface monitoring arrangement. Associated I_1 injection is not available as a synchronized continuous series in the present field dataset.

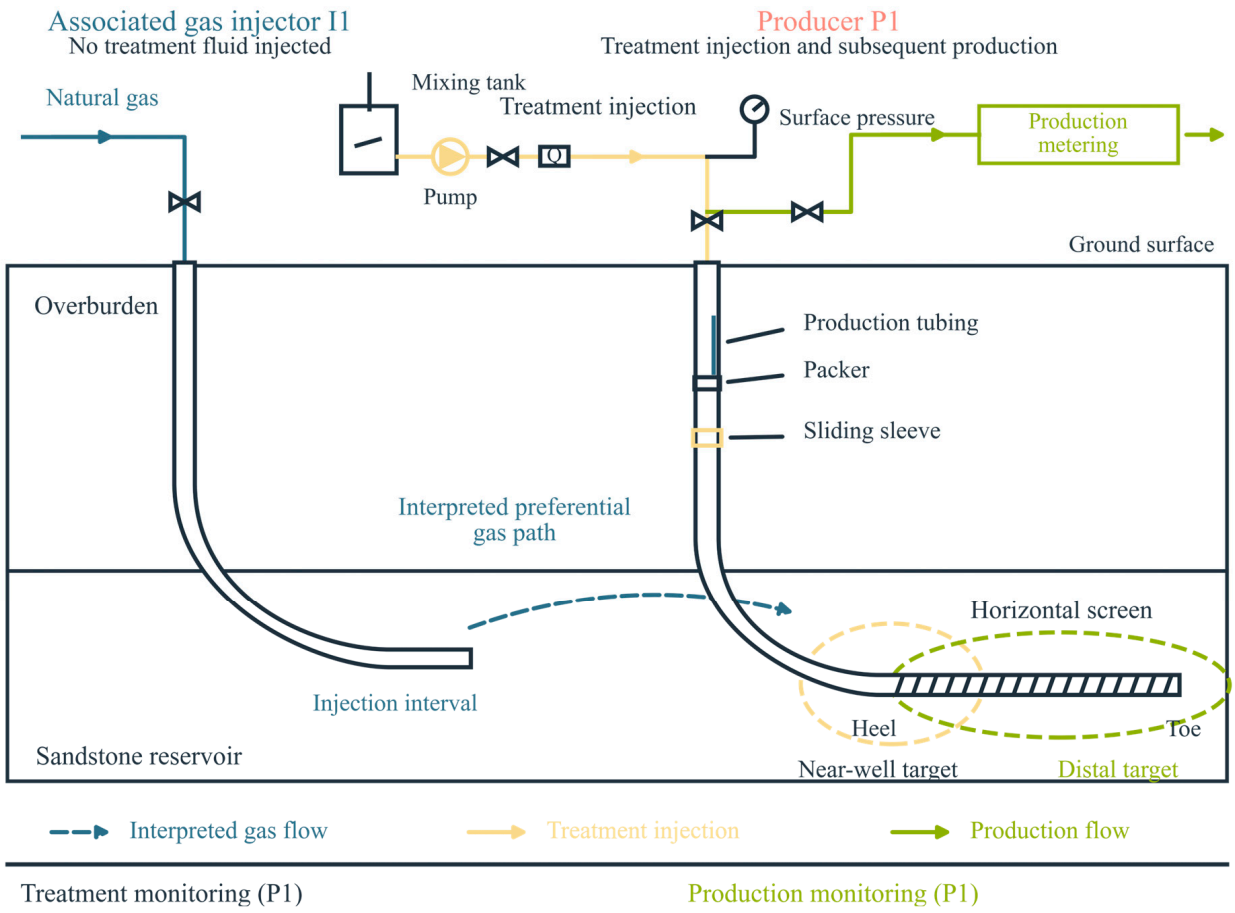


Figure 10. Well-group configuration and surface monitoring. Hardware and flow paths are schematic; treatment injection and production through P1 occur at different times. Treatment regions indicate design targets.

4.2. Pressure Response and Variable Rate Control

Both foaming fluids were injected at approximately 0.4 m^3/min. During imbibition-fluid injection, B-annulus pressure rose from 8.41 MPa at 21:08 on 28 October to 12.30 MPa at 02:00 on 29 October. The rate was then reduced from 0.4 to 0.3 m^3/min. By 04:00, B-annulus pressure had reached 13.40 MPa, and the rate was further reduced to 0.2 m^3/min. At 14:50, it was 14.00 MPa; light-oil displacement ended near 20:50 with 15.19 MPa recorded. Table 4 gives the stage checkpoints. These were trend-based operational decisions at recorded checkpoints, not a retrospectively fitted universal pressure-rise threshold. A numerical dP/dt trigger was not specified in the available procedure.

Table 4. B-annulus checkpoints and injection rate decisions.

Time	B Annulus MPa	Operational Record
28 Oct 21:08	8.41	Start of imbibition stage at approximately 0.4 m^3/min
29 Oct 02:00	12.30	Rate changed from 0.4 to 0.3 m^3/min
29 Oct 04:00	13.40	Rate changed from 0.3 to 0.2 m^3/min
29 Oct 14:50	14.00	End of imbibition-fluid injection
29 Oct 20:50	15.19	End of light-oil displacement

The 30 MPa line in Figure 11 denotes the surface injection-pressure warning specified in the P_1 treatment procedure. The job used a high-pressure manifold with a 70 MPa pressure rating, placing the operational warning below the rating of this surface component. Pressure control was coupled with injection-rate adjustment: the rate was reduced as pressure increased, and the procedure required immediate pump shutdown and inspection if pressure remained above 30 MPa after the rate had been reduced to 0.1 m^3/min. The inspection focused on restricted formation intake and tubing abnormalities before further injection. The 30 MPa setting defined the operational response threshold for this treatment, while B-annulus pressure was monitored separately to guide rate adjustment.

The recorded maxima were 29.2 MPa for pump pressure and 25.7 MPa for tubing pressure. Tubing pressure rose during early chemical injection, fell with rate reductions and later rose during light-oil displacement. These observations establish a changing surface pressure–rate response. At a fixed rate and in a comparable fluid state, a corrected rise in formation pressure drop would support increasing flow resistance; the present raw surface series cannot isolate that change. Hydrostatic head, tubing friction, fluid density, reservoir pressure and rate all contribute, and no contemporaneous downhole pressure or complete fluid-density/rheology history is available for quantitative separation. Thus, no field resistance factor is calculated. Panel (b) reports interval-average rates calculated from cumulative-volume/time records; panel (c) presents the available B-annulus checkpoints without an interpolated continuous series.

A sustained B-annulus rise was used as a feedback signal for coupled wellbore loading. Without complete annular isolation, temperature and downhole-pressure records, pressure communication, thermal response and mechanical loading cannot be separated uniquely. The checkpoints do not resolve a continuous pressure-rise slope or demonstrate a distinct causal break after either rate reduction. Thus, the annulus signal supports operational caution but does not directly locate a foam front or quantify formation resistance.

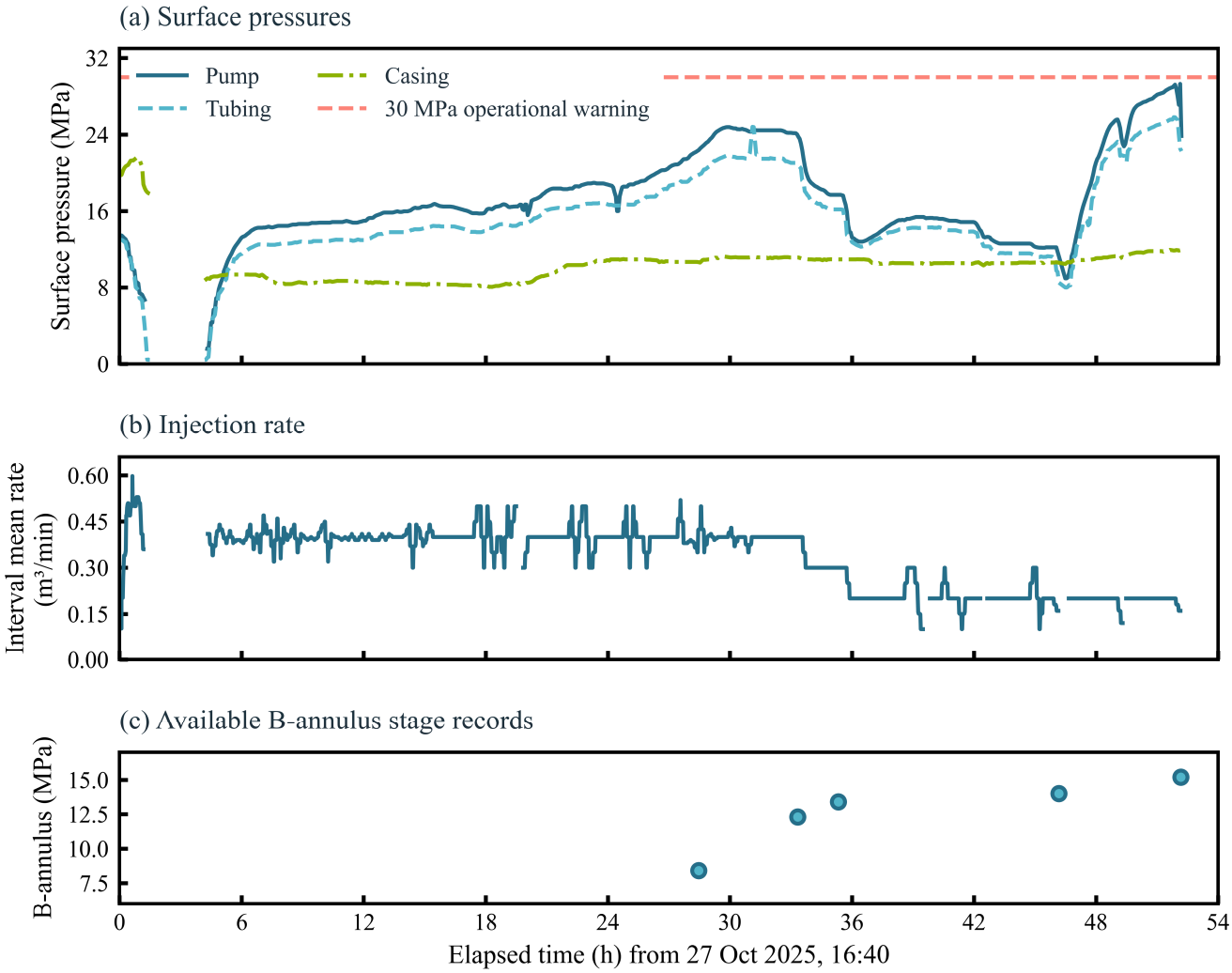


Figure 11. Surface pressure, interval-average rate and available B-annulus checkpoints during treatment. The horizontal 30 MPa line is an operational warning; pressure/rate traces are digitized, and B-annulus values are stage records.

4.3. Reporting Period Production and Endpoint Behavior

P_1 resumed natural flow after unloading and gas lift. From 1 December 2025 to 30 June 2026, inclusive, the reporting window contains 212 calendar days. Recorded cumulative oil and gas were 4030.84 t and 4,364,882 m^3. Calendar-average rates are therefore 19.01 t/d and 20,589.07 m^3/d. The cumulative-production gas–oil ratio was calculated by dividing cumulative gas production by cumulative oil production, yielding 1082.87 m^3/t; it is not the arithmetic mean of daily gas–oil ratios.

The 2022 historical reference gas–oil ratio is 5058.03 m^3/t. Relative to that reference, the period ratio decreased by 78.6%. A lower ratio does not require the absolute gas rate to fall: oil output can increase proportionally more than gas output, and additional oil from a lower-GOR flow contribution can lower the combined ratio.

On 30 June, oil and gas rates were 21.62 t/d and 37,592 m^3/d, giving 1738.76 m^3/t, 60.6% above the full-period GOR. Figure 12 shows this late increase in gas output. Possible explanations include renewed preferential gas flow, changes in neighboring injection, pressure evolution and operating adjustments.

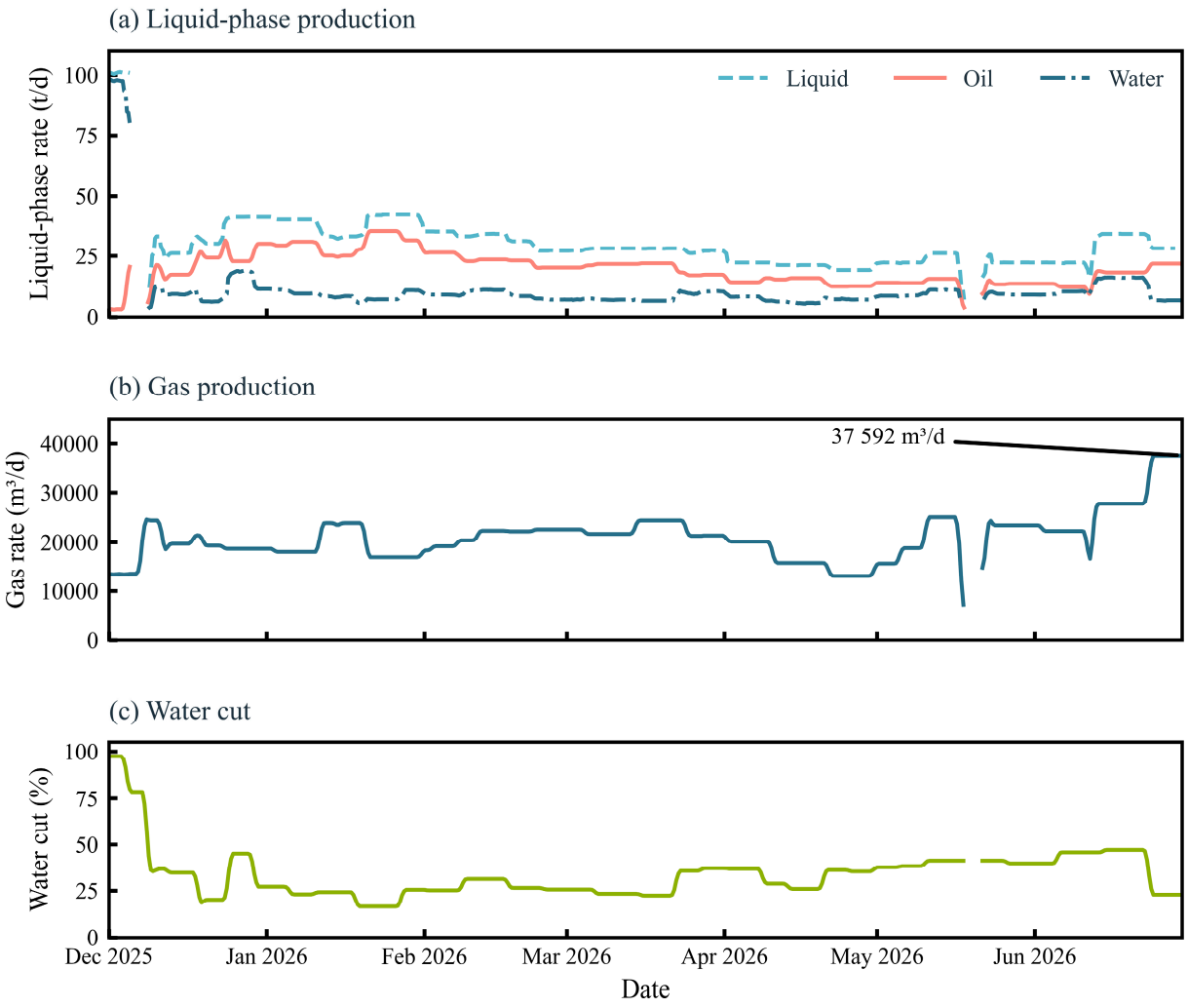


Figure 12. Liquid-phase production, gas production and water cut during the reporting period.

4.4. Historical Baseline Sensitivity

A longer immediate pretreatment baseline with comparable operating conditions was not available in the verified dataset. The retained historical reference is consequently used only for a conditional accounting calculation. If R_0 were maintained, the same gas volume would correspond to a reference oil mass of Vg/R0; the reference-equivalent increment is given in Equation (6). This construction does not reproduce the natural decline trajectory of an untreated control, account for every operational change or independently establish returned light-oil subtraction. The reported oil totals follow the source production-accounting convention; the origin of all returned oil was not separately traced.

$$\Delta M_{ref} = M_0 - \frac{V_g}{R_0} \quad (6)$$

Using R_0 = 5058.03 m^3/t gives 3167.88 t. Table 5 varies that assumed baseline by −20%, −10%, +10% and +20%, without changing the observed oil and gas totals. The resulting range is 2952.14–3311.71 t. These are hypothetical reference cases, not measured alternative baselines, confidence limits or a treatment-attribution interval. The calculation is particularly sensitive to lower reference GOR values because the counterfactual oil term increases as R_0 decreases. A different valid operating baseline could change the result beyond the illustrated range.

Table 5. Sensitivity of reference-equivalent incremental oil to the assumed baseline.

Baseline Change	Reference GOR m^3/t	Reference Oil t	Equivalent Increment t
−20%	4046.424	1078.70	2952.14
−10%	4552.227	958.85	3071.99
Adopted reference	5058.030	862.96	3167.88
+10%	5563.833	784.51	3246.33
+20%	6069.636	719.13	3311.71

A separate full-return scenario illustrates the scale of displacement-oil accounting. Using the injected 62.8 m^3 and the design density of approximately 0.85 t/m^3 gives about 53.38 t of displacement oil. If all of that inventory were recovered within the reporting window and included in the recorded oil total, it would represent about 1.32% of that total; subtracting it would reduce the reference-equivalent increment to approximately 3114.50 t. This is an inventory-based scenario, not a measurement of returned-fluid composition. It addresses only displacement oil and does not remove the effects of operating changes, neighboring injection or natural decline.

5. Discussion

5.1. Mechanism Evidence and Placement Uncertainty

The experimental evidence is strongest for a changed core-scale flow response and additional oil recovery after the composite treatment. It is weaker for the exact sequence advantage and weaker still for underground segregation into separate near and far treatment zones. Neither a static half-life nor a surface pressure curve establishes that the conventional fluid reached a fixed outer radius, the enhanced fluid remained in an inner ring and all imbibition fluid entered low-permeability rock. Actual allocation depends on completion exposure, local mobility, capillary entry, adsorption, dispersion and subsequent displacement. The geometric terms in Equation (1) and the arrows in the schematics therefore specify design allocations rather than independently observed boundaries. A reduced conductance of the gas-dominant path can redirect part of a later fluid if another connected path remains accessible. This provides a technical reason for coupling resistance development to a subsequent mobilization fluid. However, the two foam formulations can overlap and mix underground, and early resistance may also limit later access. Their balance must be verified for another well. Tracer-resolved slug arrival, segmented injectivity/production logging, downhole pressure and equal-dose sequence controls would discriminate between the proposed mechanisms. The present pilot provides operational feasibility and supporting core responses, not full spatial verification.

5.2. Comparison with Published Processes

Table 6 adds quantitative horizontal-producer benchmarks from Telin et al. [7]. Their W_2 case had no reported gas-cap inflow for about six months before recurrence; its oil rate initially fell and later recovered. W_3 showed a strong initial GOR reduction, followed by substantial gas rebound within the reported month. These histories show why endpoint and period-average metrics must be distinguished. GOR values are those reported by the authors and are not reconstructed from gas-cap inflow alone. Their materials, isolation procedures and evaluation conditions differ from those of P_1. Xiao et al. and Hassanzadeh et al. provide additional sandstone-pilot and field-delivery context [5,6], but no common-condition comparison with this 140 °C, 2.34 × 10^5 mg/L producer-side job was available.

Table 6. Published process comparison and limits of comparability.

Study	Process and Evidence	Outcome or Role	Comparison Limit
Telin et al., W_2 [7]	Self-generating foam gel followed by hydrogel; horizontal producer	Oil 9.7 → 8.5 → 10.3 t/d; reported GOR 7576 → 29 → 642 m^3/t	Before/restart 16 Sep 2022/1 Sep 2023. No gas-cap inflow for about six months; different chemistry and baseline
Telin et al., W_3 [7]	Foam-gel/hydrogel gas shutoff; horizontal producer	Oil 8.0 → 12.0 → 10.1 t/d; reported GOR 7045 → 354 → 4274 m^3/t	Before/restart 22 Aug/21 Sep 2023. Gas rebound after 2 Sep; not a 212-day matched comparison
Xiao et al. [6]	Foam-assisted deoxidized-air flooding; laboratory and sandstone pilot	Connects screening and injection organization to field response	Gas source and injection objective differ; no harmonized P1 GOR window
Hassanzadeh et al. [5]	CO_2-dissolved surfactant delivery; field foam process	Addresses delivery and sweep at field scale	Injector-side process; cannot estimate producer shutoff superiority
Shojaiepour et al. [4]	Selective foam scheduling; reservoir simulation	Evaluates placement and operating choices	Simulation evidence, not an independent field control
Present P1 pilot	Sequential aqueous fluids with surface-responsive rate control	212-day mean oil 19.01 t/d; GOR 1082.87 m^3/t	One well, historical baseline and unverified subsurface boundaries

The published foam-gel study used 60 °C and a 20.5 g/L brine model in its laboratory filtration work [7]; those test conditions must not be presented as a verified match to P_1 or as the field temperature and salinity of every reported well. The present workflow adds a documented volume-and-displacement design and pressure-responsive execution for sequential non-crosslinked aqueous fluids. It does not establish a larger GOR reduction, a greater oil-rate uplift or a longer effective life than those prior field treatments.

The specific addition is the documented link between producer-side functional staging, explicit volume assumptions, tubing displacement and pressure-responsive execution. Without a parallel control or matched conventional job, the benefit attributable specifically to staging cannot be quantified. Choke adjustment and gas lift may increase delivered oil; shut-in may redistribute pressure and saturation; neighboring injection may change gas supply; and natural decline may change the untreated oil trajectory. Their signs can depend on the operating state.

5.3. Candidate Wells and Operational Boundaries

Suitable candidates have a persistent gas-entry problem supported by production and geological evidence, remaining connected oil-bearing intervals, completion access for controlled injection and a wellbore that can tolerate the required operation. The permeability ratio of 5.26 is a laboratory example, not a mandatory field screening cutoff. The 140 °C evaluation and specified brine composition define the tested fluid envelope; higher temperature, different divalent-ion content, gas composition or oil properties require renewed compatibility and dynamic testing. Wells dominated by uncontrolled large fractures or caves require a different placement and containment assessment. Aftercare should include defined production intervals, choke and lift records and synchronized associated-injector information. Pressure safety requires a separate assessment. Rock failure depends on

pore structure and loading conditions, as discussed in studies of native pores and failure predictability [26]; such findings do not determine a safe pressure for P_1. The 30 MPa job warning cannot replace a leak-off/fracture assessment, verified annulus limits or equipment ratings. For transfer to another well, these limits and a documented response to a sustained annulus-pressure rise must be established before selecting a rate. During this pilot, the rate was reduced as the B-annulus signal increased, with the aim of limiting hydraulic loading; this response did not identify a unique downhole foam location.

5.4. Economic Potential and Engineering Implications

The field application demonstrated considerable oil-production potential and favorable prospects for economic performance. During the 212-day evaluation period, cumulative oil production reached 4030.84 t, with an average daily production rate of 19.01 t/d. The cumulative-production gas–oil ratio decreased to 1082.87 m^3/t, representing a 78.6% reduction relative to the historical reference of 5058.03 m^3/t. Based on the historical gas–oil ratio accounting method, the reference-equivalent incremental oil was estimated at 3167.88 t. Sensitivity analysis using ±20% variations in the historical reference yielded 2952.14–3311.71 t, indicating a substantial oil-production response across the examined reference scenarios.

The economic potential of the treatment can be evaluated using the attributable fraction of reference-equivalent oil, the oil netback and the total incremental treatment cost. The conditional net economic value is expressed as

$$\mathbf{\Pi} = \eta_a \mathbf{\Delta} M_{ref} b_o - C_{total} \quad (7)$$

where $\mathbf{\Pi}$ is the conditional net economic value, η_a is the assumed treatment-attribution fraction, $\mathbf{\Delta} M_{ref}$ is the reference-equivalent incremental oil, b_o is the netback per tonne of oil after applicable production charges, and C_{total} is the total incremental treatment cost, including chemicals, fluid preparation, pumping, field services, displacement oil and additional unloading operations. The corresponding break-even attribution fraction is

$$\eta_{be} = \frac{C_{total}}{\mathbf{\Delta} M_{ref} b_o} \quad (8)$$

To illustrate the potential economic scale, an assumed oil netback of CNY 2000/t is considered solely for scenario analysis. At attribution fractions of 25%, 50% and 100%, the corresponding attributable oil quantities would be 791.97, 1583.94 and 3167.88 t, supporting break-even treatment costs of approximately CNY 1.58, 3.17 and 6.34 million, respectively. Even under the lower reference-equivalent estimate of 2952.14 t, a 50% attribution assumption would support a break-even treatment cost of approximately CNY 2.95 million at the same illustrative netback. These calculations demonstrate the potentially substantial economic value of the observed production response, provided that actual treatment costs remain below the corresponding break-even thresholds.

Treatment-volume optimization provides an additional opportunity for cost control. Reservoir simulation predicted one-year incremental oil volumes of 1253, 1368 and 1427 m^3 for principal-slug volumes of 300, 400 and 500 m^3, respectively. Increasing each principal slug beyond 300 m^3 required considerably more injected fluid while delivering progressively smaller incremental oil gains. Consequently, the 300 m^3 design represents a practical compromise between treatment intensity, fluid consumption and anticipated production improvement, helping to limit unnecessary chemical and operational expenditure.

Overall, the substantial oil-production response, the 78.6% reduction in the cumulative-production gas–oil ratio and controlled treatment-fluid consumption demonstrate the promising economic potential of the staged composite-slug process. Under the illustrative oil netback of CNY 2000/t, attributable oil fractions of 50% and 100% correspond to potential oil netback values of CNY 3.17 and 6.34 million, respectively, before treatment costs.

The integration of effective gas-channeling control, enhanced oil recovery and practical treatment-volume selection provides a promising approach for economically attractive field applications in underground gas storage reservoirs.

6. Conclusions

(1) A producer-side workflow integrates conventional foaming fluid, XG-enhanced foaming fluid, a water spacer, imbibition fluid and light-oil displacement. Its engineering contribution is the coordination of functional staging, explicit liquid-inventory assumptions, tubing displacement and surface-pressure-responsive injection.

(2) In the single-core test, the conventional/enhanced pair increased recovery from 38.63% to 52.27%, a gain of 13.64 percentage points. In the parallel-core test, the sequence additionally containing a spacer and imbibition fluid increased system recovery from 19.44% to 41.39%, a gain of 21.95 percentage points. Additional oil from the lower-permeability branch supports a redistribution interpretation under the tested conditions. These different tests do not isolate the benefit of staging or imbibition.

(3) The empirical inventory calculation and conditional model cases supported a case-specific target of 300 m^3 per principal slug. Actual principal-fluid volumes were 287, 288 and 288.6 m^3. Surface-pressure monitoring supported rate adjustment, while the available measurements could not determine formation resistance or underground slug boundaries.

(4) The field application demonstrated substantial production improvement and promising economic potential. Over 212 days, cumulative oil production reached 4030.84 t, averaging 19.01 t/d, while the cumulative-production gas–oil ratio decreased by 78.6% relative to the historical reference. Reference-equivalent incremental oil reached 3167.88 t. At an illustrative oil netback of CNY 2000/t, attributable oil fractions of 50% and 100% correspond to potential oil netback values of approximately CNY 3.17 and 6.34 million, respectively, before treatment costs. Combined with controlled treatment-fluid consumption, these results highlight the considerable economic potential and promising field applicability of the proposed process.

Author Contributions: Conceptualization, X.Z. and W.W.; methodology, X.Z., X.L. and J.Y.; investigation, X.Z., X.L. and Y.Z.; data curation, X.Z. and J.Y.; formal analysis, X.Z. and W.W.; visualization, X.Z.; writing—original draft preparation, X.Z.; writing—review and editing, W.W., X.L., J.Y. and Y.Z.; supervision, W.W.; project administration, W.W. All authors have read and agreed to the published version of the manuscript.

Funding: This research received no external funding.

Data Availability Statement: The data supporting the findings of this study are available from the corresponding author upon reasonable request. The field operational and production data are not publicly available due to confidentiality restrictions and may be provided subject to approval by the data owner.

Acknowledgments: The authors gratefully acknowledge the technical support provided by the field engineering and production teams during the design and implementation of the pilot treatment. The authors also thank the laboratory and reservoir-engineering personnel for their assistance with fluid preparation, field monitoring, production-data collection and post-treatment evaluation.

Conflicts of Interest: Authors Xiaocen Liu and Jie Yao were employed by PetroChina Tarim Oilfield Company. Author Yufeng Zhao was employed by Shenzhen Greending New Energy Technology Development Co., Ltd. The remaining authors declare that the research was conducted in the absence of any commercial or financial relationships that could be construed as potential conflicts of interest.

List of Symbols

Q	Treatment-fluid volume (m^3)
r_1	Equivalent treatment depth around the horizontal completion (m)
r_w	Wellbore radius (m)
d_1	Equivalent radial scale of the near-wellbore treatment region (m)
L_1	Effective fluid-intake length of the horizontal completion (m)
ϕ_1	Effective porosity of the near-wellbore treatment region
A	Engineering correction factor for the near-wellbore treatment region
r_2	Equivalent radius of the principal gas-channeling region (m)
L_2	Assigned penetration depth of the corresponding treatment slug (m)
ϕ_2	Effective porosity of the principal gas-channeling region
B	Engineering correction factor for the gas-channeling region

References

1. Jiang, T.; Qi, H.; Wang, Z.; Li, Y.; Wang, J.; Liu, Z.; Cao, J. Microscopic simulation experiment on efficient construction of underground gas storages converted from water-invaded gas reservoirs. *Pet. Explor. Dev.* **2024**, *51*, 182–189. [CrossRef]
2. Zhang, M.; Zhao, F.; Lyu, G.; Hou, J.; Song, L.; Feng, H.; Zhang, D. Experimental study on the adaptation limit of WAG to improve CO2 flooding effect. *Oilfield Chem.* **2020**, *37*, 279–286. [CrossRef]
3. Wang, G. Carbon dioxide capture, enhanced-oil recovery and storage technology and engineering practice in Jilin Oilfield, NE China. *Pet. Explor. Dev.* **2023**, *50*, 219–226. [CrossRef]
4. Shojaiepour, M.; Rashidi, F.; Dabir, B.; Amirsardari, M. A treatment protocol for controlling gas oil ratio in heterogeneous carbonate reservoirs by foam injection: Case study simulation. *J. Pet. Sci. Eng.* **2022**, *208*, 109727. [CrossRef]
5. Hassanzadeh, A.; Katiyar, A.; Kalaei, H.; Pecore, D.; Schofield, E.; Nguyen, Q.P. A novel foam process with CO2 dissolved surfactant for improved sweep efficiency in EVGSAU field. *Geoenergy Sci. Eng.* **2023**, *231*, 212310. [CrossRef]
6. Xiao, W.; Ren, J.; Pu, W.; Yuan, C.; Meng, L.; Zheng, L.; Zhao, H.; Cheng, Q. Laboratory tests and field pilot of foam-assisted deoxidized-air flooding in a low-permeability sandstone reservoir. *Fuel* **2023**, *352*, 129150. [CrossRef]
7. Telin, A.; Karazeev, D.; Vezhnin, S.; Strizhnev, V.; Levadsky, A.; Mamykin, A.; Lenchenkova, L.; Yakubov, R.; Fakhreeva, A.; Akhmetov, A.; et al. Use of self-generating foam gel composition with subsequent injection of hydrogel to limit gas inflow in horizontal wells of Vostochno-Messoyakhskoye Field. *Gels* **2024**, *10*, 215. [CrossRef] [PubMed]
8. Liu, X.; Wang, B.; Guo, C. Performance evaluation of polymer enhanced foam system and core flow characteristics. *Oilfield Chem.* **2024**, *41*, 122–130. [CrossRef]
9. Le, V.S.; Sharma, K.V.; Hanamertani, A.S.; Youssif, M.I.; Elkhatib, O.; Rane, K.; Piri, M.; Katiyar, A.; Nagarajan, N. Methane foam performance in oil-wet unconsolidated porous media: A systematic experimental investigation at reservoir conditions. *Fuel* **2023**, *344*, 128002. [CrossRef]
10. Hussain, A.A.A.; Vincent-Bonnieu, S.; Kamarul Bahrim, R.Z.; Pilus, R.M.; Rossen, W.R. Impact of crude oil on pre-generated foam in porous media. *J. Pet. Sci. Eng.* **2020**, *185*, 106628. [CrossRef]
11. Cao, C.; Xu, S.; Zhao, Y.; Wang, Y.; Zhang, L.; Li, Q.; Zhou, S.; Wen, S.; Wei, Y.; Li, J.; et al. Transport mechanisms of CO2/N2-CH4 flow: A digital rock study based on in-situ reaction of CO2-brine-carbonate systems. *Energy* **2026**, *344*, 139772. [CrossRef]
12. Luo, J.; Wang, L. Research on gas channeling identification method for gas injection development in high-pressure heterogeneous reservoir. *Processes* **2022**, *10*, 2366. [CrossRef]
13. Zhang, L.; Wang, X.; Wu, J.; Wu, H.; Huang, S.; Liu, X. Gas channeling identification in fractured condensate gas reservoirs: Methodology and application. *ACS Omega* **2025**, *10*, 44596–44607. [CrossRef] [PubMed]
14. Fritis, G.C.; Paz, P.S.Z.; Chapiro, G. Modeling the optimal foam injection slug in porous medium accounting adsorption effects. *Int. J. Non-Linear Mech.* **2025**, *178*, 105199. [CrossRef]
15. Bouquet, S.; Douarche, F.; Roggero, F.; Bourbiaux, B. Foam processes in naturally fractured carbonate oil-wet reservoirs: Technical and economic analysis and optimization. *J. Pet. Sci. Eng.* **2020**, *190*, 107111. [CrossRef]
16. Huang, W.; Wen, R.; Pang, J.; Sun, Y.; Yang, W. Experiment on injection parameter optimization for air foam flooding in low-permeability heterogeneous reservoir. *Spec. Oil Gas Reserv.* **2021**, *28*, 124–129. [CrossRef]
17. Chen, H.; Yang, R.; Liu, X.; Tan, X.; Tian, X.; Li, B. Performance of anti-gas-channeling polymer foam system in high temperature low permeability reservoir. *Oilfield Chem.* **2022**, *39*, 295–300. (In Chinese) [CrossRef]
18. Xu, D.; Li, Z.; Bai, B.; Chen, X.; Wu, H.; Hou, J.; Kang, W. A systematic research on spontaneous imbibition of surfactant solutions for low permeability sandstone reservoirs. *J. Pet. Sci. Eng.* **2021**, *206*, 109003. [CrossRef]
19. Gong, J.-K.; Wang, Y.; Kamarul Bahrim, R.-Z.B.; Tewari, R.-D.; Mahamad Amir, M.-I.; Farajzadeh, R.; Rossen, W. Liquid injectivity in a SAG foam process: Effect of permeability. *Pet. Sci.* **2024**, *21*, 302–314. [CrossRef]

20. Saifullin, E.R.; Nazarychev, S.A.; Zharkov, D.A.; Malahov, A.O.; Varfolomeev, M.A.; Yuan, C.; Zhanbossynova, S.; Zvada, M.V.; Belovus, P.N. Coreflood testing of gas-blocking agents: Selectivity in high-heterogeneity reservoirs and efficiency in low-temperature conditions. *Energy Fuels* **2023**, *37*, 11720–11729. [CrossRef]
21. Zhang, B.; Nie, F.; Deng, X.; Wang, Y.; Hou, B. Evaluation of an oxygen-reduced air flooding plugging system and its injection method in the Honghe Oilfield. *Energy Fuels* **2022**, *36*, 12524–12532. [CrossRef]
22. Chen, Z.; Wang, L.; Luo, J.; Zhang, J. Visualization and simulation of foam-assisted gas drive mechanism in surface karst slit-hole type reservoirs. *Processes* **2024**, *12*, 2579. [CrossRef]
23. Gu, X.; Cai, G.; Fan, X.; He, Y.; Huang, F.; Gao, Z.; Kang, S. Evaluation of foam gel compound profile control and flooding technology in low-permeability reservoirs. *Processes* **2023**, *11*, 2424. [CrossRef]
24. Fan, X.; Zhou, J.; Zhou, Y.; Zhang, J.; Zhang, X. An experimental of "enhanced foam + gel" flooding in high salinity reservoirs. *J. Southwest Pet. Univ. (Sci. Technol. Ed.)* **2024**, *46*, 159–168. [CrossRef]
25. Li, D.; Saraji, S.; Jiao, Z.; Zhang, Y. An experimental study of CO2 injection strategies for enhanced oil recovery and geological sequestration in a fractured tight sandstone reservoir. *Geoenergy Sci. Eng.* **2023**, *230*, 212166. [CrossRef]
26. Wang, L.; Hao, Q.; Zhong, Y.; Liu, X.; Xie, Q.; Tian, X.; Qin, F. Influence of native pores on the size distribution and predictability of rock failure. *J. Rock Mech. Geotech. Eng.* **2026**, *18*, 1447–1459. [CrossRef]

Disclaimer/Publisher's Note: The statements, opinions and data contained in all publications are solely those of the individual author(s) and contributor(s) and not of MDPI and/or the editor(s). MDPI and/or the editor(s) disclaim responsibility for any injury to people or property resulting from any ideas, methods, instructions or products referred to in the content.